JIRBDAI

Journal of Institutional Research, Big Data Analytics and Innovation

COMPARISON OF METHODS IN THE SPECTRAL NUMERICAL ANALYSIS OF MAGNETO-CONVECTIVE VISCOELASTIC BIOFLUID FLOW THROUGH PORO-ELASTIC MEDIA

Osho Femi Timothy[1,2], Moses Felix Oghenerobor[1], Adetokunbo Blessing Oluwatosin[1]

[1]Department of Mathematics, Adeyemi Federal University of Education, Ondo State, Nigeria.
[2]Department of Mathematics and Statistics, Redeemer's University, Ede, Nigeria,
[1]oshoft@aceondo.edu.ng, [2]felixoghene9@gmail.com , [3]adetokunboblessing05@gmail.com,

ABSTRACT This study presents a comparative analysis of three numerical methods- Spectral Quasi-Linearization Method (SQLM), Spectral Chebyshev Collocation Method (SCCM) and the Shooting Runge-Kutta (Shooting RK4)- for the spectral numerical analysis of magneto-convective viscoelastic biofluid flow through poroelastic media. The research focuses on the efficacy, accuracy, and computational efficiency of each method in solving the complex governing equations of magneto-convective viscoelastic biofluid dynamics in porous and elastic environments. Through a series of benchmark problems, the performance of each method is evaluated in terms of convergence rates, error analysis, and computational cost. The results provide valuable insights into the suitability and limitations of these methods for simulating biofluid flows in biomedical and engineering applications. The findings suggest optimal scenarios for the application of each method, contributing to the advancement of numerical techniques in the study of magneto-convective viscoelastic flows in poroelastic media.

KEYWORDS: Magnetohydrodynamics, viscoelastic biofluid, Poro-elastic medium, convective flow.

I. INTRODUCTION

Significant advancements in flow and heat transfer via a deformable porous media have been realized in recent years. A strong framework for comprehending the relationship between fluid flow and solid deformation in porous media is provided by photoelasticity. It has uses in a variety of fields, including biomedical engineering and geomechanics. A system of coupled equations describing fluid-solid interaction in porous media was established by Biot (1941, 1956). Effective stress and fluid saturated wave velocities were discussed by Gassmann (1951), and Stephansson (2003) used poroelastic modeling to shed light on fluid-induced seismicity. While Coussy (2004) created extensive poroelastic frameworks for engineering applications, Mow et al. (1980) used poroelasticity to evaluate the flow-dependent viscoelastic properties of articular cartilage. In order to take microstructure effects in poroelasticity into consideration, Borja and Koliji (2009) investigated hierarchical models. The inquiry of the electronic component convection flow has been a focal point in various articles over the past decade. In their work, Baskaya et al. (2005) studied convective heat transmission in a rectangular channel from a variety of isolated heat sources. Bhowmik et al. (2005) carried out steady state experiments using water as the working fluid in a rectangular vertical channel. A range of isolated heat sources led to an improvement in heat transmission, which was linked to the onset of instability and an increase in buoyancy-induced secondary flow. Their experimental outcomes

led to the proposal of experimental relationships among Nu, Re, and Gr. Choi and Kim (1996) conducted a numerical investigation into 3D conjugate mixed convection heat transfer in a rectangular channel, with several flow regimes defined by a modified 5% rule. Culham *et al.* (1997) conducted a comprehensive examination of existing models and correlations for mixed and natural convective heat transfer in a parallel plate channel that is heated uniformly and vertically. Ermolaev and Zhbanov (2004) employed Mixed convection heat transport in a horizontal channel is analyzed using numerical solutions of 2D, unstable Navier-Stokes equations. The Boussinesq approximation is used, and the Galerkin finite element method is used to get solutions.

Entropy production and heat line visualization analysis on time-dependent free convection flow of a second-grade elastic-viscous fluid have been studied in studies like those by Kumar et al. (2019) and Adesanya et al. (2017) on third-grade Reiner-Rivlin fluids with chemical processes. Biophysical fluids are frequently represented using the Jeffrey fluid model, a flexible nonlinear viscoelastic hydrodynamic model. Researchers have recognized the limitations of using Navier-Stokes equations to simulate such complex fluids, leading to the exploration of a wide range of models for viscoelastic fluids. These models incorporate distinct properties of the material, such as variations in normal stress, elasticity, viscosity, relaxation durations, and retardation. Thermodynamic optimization has shown interest in biological and industrial liquids, including blood, due to their heat-conducting properties. The Jeffrey fluid model, a versatile nonlinear viscoelastic hydrodynamic model, has been widely used to represent biophysical fluids, with studies by Varjravelu *et al.* (2011) and Tripathi and Beg (2013) highlighting its applicability.

The Magnetohydrodynamics (MHD) convective flow of a nanofluid in a lid-driven porous enclosure with non-uniform thermal vertical walls under the impact of heat radiation was studied by Muthukumar *et al.* (2019). Consequently, numerous studies have explored minimizing entropy generation in the realm of biological magnetothermal fluid dynamics. Beg *et al.* (2013) employed a homotropy technique to calculate the Bejan number and entropy generation rates in magnetized biofluid transport from a rotating disk. Khan *et al.* (2019) conducted an analysis on the entropy generation rate in thin film reactive mixed convection magnetohydrodynamic viscoelastic nanofluid 14 bioconvection within a Darcian porous regime. The interaction of the creation of entropy by radiative heat transport has garnered attention as well. Ramana Murthy *et al.* (2017) explored impacts of thermal radiation on heat transfer and entropy formation in dual immiscible non-Newtonian Stokes pair stress fluids, revealing a reduction in thermal radiation and entropy production and an enhancement with dissipation of viscosity.

This work introduces a comprehensive comparative analysis of spectral numerical methods for modeling magneto-convective viscoelastic biofluid flow through poro-elastic media, a topic of significant importance in biomedical and industrial applications. The novelty lies in the following contributions:

a) Innovative coupling of physical phenomena
b) Spectral numerical methodology
c) Benchmarking against analytical solutions
d) Practical insights for application d to represent biophysical fluids.

This work lays the groundwork for further advancements in biofluid dynamics and engineering applications by substantially expanding the numerical modeling toolkit available to researchers studying magneto-convective viscoelastic flow in porous environments. Innovative physical phenomenon connection; spectral numerical methodology; comparison with analytical solutions; and useful application insights for biophysical fluid representation.

II. MODEL FOR MAGNETO-VISCOELASTIC TRANSPORT IN DEFORMABLE MEDIUM

Mallikarjuna et al (2021)

$$\mu \frac{d^2U}{dY^2} - (1-\phi)\frac{dP}{dX} + KV = 0 \qquad (1)$$

Government elastic equilibrium equation.

From dimensionless variables,

$$y=\frac{Y}{h},x=\frac{X}{h},v=\frac{2\mu_a V}{\rho g\beta h^2\left(T_1-T_0\right)},u=\frac{\mu U}{\rho g\beta h^2\left(T_1-T_0\right)}\theta=\frac{T-T_0}{T_1-T_0},p=\frac{P}{\rho g\beta h\left(T_1-T_0\right)}$$

Substituting the dimensionless variable into equation (1), to have

$$\frac{d^2u}{dy^2}-(1-\phi)\frac{dp}{dx}+\delta v=0 \qquad (2)$$

From $\delta = Kh^2$, we have

$$\frac{2\mu_a}{1+\lambda_1}\frac{d^2V}{dY^2}-\phi\frac{dP}{dX}-KV-\sigma B_0^2V+\rho g\beta\left(T-T_0\right)=0 \qquad (3)$$

Momentum Conservation Equation.

Substituting the dimensionless variables into equation (3),

Where $M=B_0h\sqrt{\frac{\sigma}{2\mu_a}}$ and $\delta=\frac{kh^2}{2\mu_a}$, to have

$$\frac{1}{(1+\lambda_1)}\frac{d^2v}{dy^2}-\phi\frac{dp}{dx}-\ \delta v-M^2v+\theta=0 \qquad (4)$$

Heat Equation

$$\frac{K_0}{\rho c_\rho}\frac{d^2T}{dY^2}+\frac{2\mu_a}{(1+\lambda_1)\rho c_\rho}\left(\frac{dV}{dY}\right)^2-\frac{1}{\rho c_\rho}\frac{dq_r}{dY}+\frac{KV^2}{\rho c_\rho}=0 \qquad (5)$$

Where $y=\frac{Y}{h},v=\frac{2\mu_a V}{\rho g\beta h^2\left(T_1-T_0\right)},\ \theta=\frac{T-T_0}{T_1-T_0},\ \frac{dy}{dx}=\frac{-16\sigma^*T_1^3d^2T}{3K^*dY^2}$

Substitute these into equation (5), to have

$$\left(1+\frac{4}{3}R\right)\frac{d^2\theta}{dy^2}+\frac{N}{1+\lambda_1}\left(\frac{dv}{dy}\right)^2+N\delta v^2=0 \qquad (6)$$

The boundary conditions are:

$$\left.\begin{array}{l} \frac{dU}{dY} = 0, \frac{dV}{dY} = 0, \frac{dT}{dY} = 0 \, at \, Y = 0 \\ U = 0, V = 0, T = T_1 \, at \, Y = h \end{array}\right] \quad (7)$$

we arrived at the governing elastic equilibrium equation,

$$\frac{d^2u}{dy^2} - (1-\phi)\frac{dp}{dx} + \delta v = 0 \quad (2)$$

Also, the momentum conservation equation,

$$\frac{1}{(1+\lambda_1)}\frac{d^2v}{dy^2} - \phi\frac{dp}{dx} - \delta v - M^2 v + \theta = 0 \quad (4)$$

And the heat equation,

$$\left(1+\frac{4}{3}R\right)\frac{d^2\theta}{dy^2} + \frac{N}{1+\lambda_1}\left(\frac{dv}{dy}\right)^2 + N\delta v^2 = 0 \quad (6)$$

The associated boundary conditions are:

$$u = 0, v = 0, \theta = 1 at \, y = 1 \quad (8)$$

$$\frac{du}{dy} = \frac{dv}{dy} = \frac{d\theta}{dy} = 0 \, at \, y = 0 \quad (9)$$

Spectral Quasi-Linearization Method Numerical Solution

The set of nonlinear coupled Equations (2), (4), and (6) with boundary condition equations (8) and (9) is solved numerically using the Spectral Quasi-linearization Method.

$$a_{1,1}^2 u_{r+1}^{II} + a_{1,1}^1 u_{r+1}^{I} + a_{1,1}^0 u_{r+1} + a_{1,2}^0 v_{r+1} = R_1 \quad (10)$$

$$a_{2,2}^2 v_{r+1}^{II} + a_{2,2}^0 v_{r+1}^{I} + a_{2,3}\theta_{r+1} = R_2 \quad (11)$$

$$a_{3,3}^2 v_{r+1}^{II} + a_{3,2}^1 \theta_{r+1}^{I} = R_3 \quad (12)$$

The boundary conditions become

$$u_{r+1}^{I} = v_{r+1}^{I} = \theta_{r+1}^{I} = 0 \, at \, y = 0 \quad (13)$$

$$u_{r+1} = v_{r+1} = \theta_{r+1} = 1 at \, y = 1 \quad (14)$$

The featured coefficients in equations (10) – (12) are:

$$a_{1,1}^2 = 1, a_{1,1}^1 = 0, a_{1,2}^0 = 0, a_{1,2}^0 = \delta$$

$$a_{2,2}^2 = 1, a_{2,2}^0 = -(1+\lambda_1)(\delta + M^2), a_{2,3}^0 = (1+\lambda_1)$$

$$a_{3,3}^2 = 1 + \frac{4}{3}R, a_{3,2}^1 = \frac{N}{1+\lambda_1} 2v_{1,}^I \quad a_{3,2}^1 = N\delta 2v_r$$

$$R_1 = (1-\phi)P, R_2 = \phi(1+\lambda_1), and\ R_3 = \frac{N}{1+\lambda_1}(v_r^I)^2 + N\delta v_r^2 \qquad (15)$$

III. RESULTS AND DISCUSSION

The results obtained from the spectral numerical study of magneto-convective viscoelastic biofluid flow through poro-elastic media will be presented. The discussion of the results will shed light on the behavior and characteristics of the flow and the effect of various parameters involved. Tables 1-10 captures the validation of numerical results for solid displacement, flow velocity and volume fraction of the fluid.

Table 1: SCM and Shooting RK4 for Solid Displacement

Y	u(y)-SCM	u(y)-Shooting-RK4	Absolute Error
0	0.4092355332574184	0.40923554286302094	$9.60560253560061 \times 10^{-9}$
0.1	0.40477884291462063	0.40477884487969573	$1.965075102638991 \times 10^{-9}$
0.2	0.3914498602689724	0.39144986454133396	$4.272361575630157 \times 10^{-9}$
0.3	0.36937277597898843	0.36937278282526625	$6.84627782243652 \times 10^{-9}$
0.4	0.33875768085692787	0.33875769050130444	$9.644376575135283 \times 10^{-9}$
0.5	0.2999053003390014	0.2999053107463026	$1.040730118750943 \times 10^{-8}$
0.6	0.25321377316787763	0.2532137856420392	$1.247416159255721 \times 10^{-8}$
0.7	0.19918762605846557	0.1991876410509502	$1.499248461489521 \times 10^{-8}$
0.8	0.138449141085021	0.1384491590001712	$1.791515022442347 \times 10^{-8}$
0.9	0.07175235809515387	0.07175237913648216	$2.104132829083838 \times 10^{-8}$
1	$8.085663848046625 \times 10^{-18}$	$2.469566836884631 \times 10^{-8}$	$2.469566836076065 \times 10^{-8}$

Ny=30; δ=1; H=1; ϕ=0.6; G=-1; λ_1=0.2; R=1; m=1

Table 2: SCM and Shooting RK4 for Velocity

Y	v(y)-SCM	v(y)- Shooting-RK4	Absolute Error
0	0.49202082586110873	0.49202083397566904	$8.114560301475393 \times 10^{-9}$
0.1	0.48791967648689993	0.4879196731590484	$3.327851549883576 \times 10^{-9}$
0.2	0.4755238550201703	0.4755238461284732	$8.891697100832374 \times 10^{-9}$
0.3	0.45455410827515325	0.4545540931082821	$1.516687114788695 \times 10^{-8}$
0.4	0.42453788519490765	0.42453786331015003	$2.188475761721875 \times 10^{-8}$
0.5	0.3847985813316363	0.3847985573303162	$2.400132009805489 \times 10^{-8}$
0.6	0.33444036885219514	0.3344403399625362	$2.888965894287665 \times 10^{-8}$
0.7	0.27232852818285236	0.2723284935209219	$3.466193043699661 \times 10^{-8}$
0.8	0.1970652178929411	0.19706517684523636	$4.104770473523089 \times 10^{-8}$
0.9	0.10696068038929912	0.10696063224109972	$4.814819939968906 \times 10^{-8}$
1	$1.487248760119362 \times 10^{-17}$	$-5.607540779544118 \times 10^{-8}$	$5.607540781031367 \times 10^{-8}$

$Ny = 30; \delta = 1; H = 1; \phi = 0.6; G = -1; \lambda_1 = 0.2; R = 1; m = 1$

Table 3: SCM and Shooting RK4 for Temperature

Y	Θ (y)-SCM	Θ (y)- Shooting-RK4	Absolute Error
0	1.0662875289090126	1.066287547424466	$5.03298114296058 \times 10^{-9}$
0.1	1.0657682129138761	1.0657682295766935	$5.119088930527482 \times 10^{-9}$
0.2	1.0642031492696786	1.0642031622300614	$4.269768760778447 \times 10^{-9}$
0.3	1.0615682932420807	1.0615683010735861	$2.953535549465869 \times 10^{-8}$
0.4	1.0578142855452053	1.0578142863000166	$3.212274091168865 \times 10^{-8}$
0.5	1.0528514760594918	1.0528514766537338	$7.434007409656829 \times 10^{-9}$
0.6	1.0465267616092888	1.0465267580744422	$1.086123517790582 \times 10^{-7}$
0.7	1.0385898096924673	1.0385897992617728	$1.529545590184255 \times 10^{-7}$
0.8	1.0286451981233322	1.0286451784135675	$5.30024995004652 \times 10^{-8}$
0.9	1.0160856707147763	1.0160856444742878	$6.441063593598528 \times 10^{-8}$
1	1.0000000000000002	0.9999999667115499	$6.368073557361242 \times 10^{-8}$

$Ny = 30;\ \delta = 1;\ H = 1;\ \phi = 0.6;\ G = -1;\ \lambda_1 = 0.2;\ R = 1;\ m = 1$

Table 4: SQLM and SCM for Solid Displacement

Y	u (y)-SQLM	u (y)- SCM	Absolute Error
0	0.409235533256931	0.4092355332574184	$1.851545339270899 \times 10^{-8}$
0.1	0.404778840588483	0.40477884291462063	$1.666281734813424 \times 10^{-8}$
0.2	0.391449858196354	0.3914498602689724	$1.296038276699107 \times 10^{-8}$
0.3	0.369372717082718	0.36937277597898843	$7.831505444144682 \times 10^{-9}$
0.4	0.338757626351711	0.33875768085692787	$7.548113245547938 \times 10^{-10}$
0.5	0.299905300338649	0.2999053003390014	$5.942419889493067 \times 10^{-10}$
0.6	0.253213702036002	0.25321377316787763	$3.534846637620603 \times 10^{-9}$
0.7	0.199187541813046	0.19918762605846557	$1.043069453032785 \times 10^{-8}$
0.8	0.138449136203938	0.138449141085021	$1.970976470921925 \times 10^{-8}$
0.9	0.071752353590178	0.07175235809515387	$2.624048844879212 \times 10^{-8}$
1.0	$-4.821663901477535 \times 10^{-15}$	$8.085663848046625 \times 10^{-18}$	$3.328845032957161 \times 10^{-8}$

$Ny = 30;\ \delta = 1;\ H = 1;\ \phi = 0.6;\ G = -1;\ \lambda_1 = 0.2;\ R = 1;\ m = 1$

Table 5: SQLM and SCM for Velocity

Y	v (y)-SQLM	v (y)- SCM	Absolute Error
0	0.49202082585997	0.49202082586110873	$1.138755756358023 \times 10^{-12}$
0.1	0.487919681716172	0.48791967648689993	$5.229272070916835 \times 10^{-9}$
0.2	0.475523859673885	0.4755238550201703	$4.65371469138276 \times 10^{-9}$,
0.3	0.454554240908597	0.45455410827515325	$1.326334437279364 \times 10^{-7}$
0.4	0.424538007969754	0.42453788519490765	$1.227748463450417 \times 10^{-7}$
0.5	0.384798581330831	0.3847985813316363	$8.053002709118573 \times 10^{-13}$
0.6	0.334440527642153	0.33444036885219514	$1.587899578492368 \times 10^{-7}$
0.7	0.272328715385062	0.27232852818285236	$1.87202209622761 \times 10^{-7}$
0.8	0.197065228326544	0.1970652178929411	$1.043360289831873 \times 10^{-8}$
0.9	0.106960690152806	0.10696068038929912,	$9.76350687798 \times 10^{-9}$
1.0	$-9.765920711002352 \times 10^{-13}$	$1.487248760119362 \times 10^{-17}$	$9.766069435878363 \times 10^{-13}$

$\mathrm{Ny} = 30; \delta = 1; H = 1; \phi = 0.6; G = -1; \lambda_1 = 0.2; R = 1; m = 1$

Table 6: SQLM and SCM for Temperature

Y	Θ (y)-SQLM	Θ (y)- SCM	Absolute Error
0	1.066287528908974	1.0662875289090126	$3.863576125695545 \times 10^{-14}$
0.1	1.065768213396178	1.0657682129138761	$4.823019761346359 \times 10^{-10}$
0.2	1.064203149333608	1.0642031492696786	$6.392930629317561 \times 10^{-11}$
0.3	1.061568318963338	1.0615682932420807	$2.572125734623398 \times 10^{-8}$
0.4	1.057814314195811	1.0578142855452053,	$2.865060566570321 \times 10^{-8}$
0.5	1.052851476059487	1.0528514760594918	$4.884981308350689 \times 10^{-15}$
0.6	1.04652685599369	1.0465267616092888	$9.438440118358926 \times 10^{-8}$
0.7	1.038589938152717	1.0385898096924673	$1.284602497708675 \times 10^{-7}$
0.8	1.028645211531815	1.0286451981233322	$1.340848276853989 \times 10^{-8}$
0.9	1.016085681185261	1.0160856707147763	$1.047048470148581 \times 10^{-8}$
1.0	0.999999999999989	1.0000000000000002	$1.121325254871408 \times 10^{-14}$

$\mathrm{Ny} = 30;\ \delta = 1;\ H = 1;\ \phi = 0.6;\ G = -1;\ \lambda_1 = 0.2;\ R = 1;\ m = 1$

Table 7: SQLM and Shooting RK4 for Solid Displacement

Y	u (y)-SQLM	u (y)- Shooting- RK4	Absolute Error
0	0.409235533256931	0.40923554286302094	$9.60608992350842 \times 10^{-9}$
0.1	0.404778840588483	0.40477884487969573	$4.291212718499082 \times 10^{-9}$
0.2	0.391449858196354	0.39144986454133396	$6.344979985861698 \times 10^{-9}$
0.3	0.369372717082718	0.36937278282526625	$6.574254823865644 \times 10^{-8}$
0.4	0.338757626351711	0.33875769050130444	$6.414959341505266 \times 10^{-8}$
0.5	0.299905300338649	0.2999053107463026	$1.04076536278086 \times 10^{-8}$
0.6	0.253213702036002	0.2532137856420392	$8.360603720447557 \times 10^{-8}$
0.7	0.199187541813046	0.1991876410509502	$9.923790419974488 \times 10^{-8}$
0.8	0.138449136203938	0.1384491590001712	$2.279623320666779 \times 10^{-8}$
0.9	0.071752353590178	0.07175237913648216	$2.554630416928827 \times 10^{-8}$
1.0	$-4.821663901477535 \times 10^{-15}$	$2.469566836884631 \times 10^{-8}$	$2.469567319051021 \times 10^{-8}$

$\mathrm{Ny} = 30;\ \delta = 1;\ H = 1;\ \phi = 0.6;\ G = -1;\ \lambda_1 = 0.2;\ R = 1;\ m = 1$

Table 8: SQLM and Shooting RK4 for Velocity

Y	v (y)-SQLM	v (y)- Shooting- RK4	Absolute Error
0	0.49202082585997	0.4092355332574184	$8.115699057231751 \times 10^{-9}$
0.1	0.487919681716172	0.40477884291462063	$8.557123620800411 \times 10^{-9}$
0.2	0.475523859673885	0.3914498602689724	$1.354541179221513 \times 10^{-8}$
0.3	0.454554240908597	0.36937277597898843	$1.478003148758233 \times 10^{-7}$
0.4	0.424538007969754	0.33875768085692787	$1.446596039622605 \times 10^{-7}$
0.5	0.384798581330831	0.2999053003390014	$2.400051479778398 \times 10^{-8}$
0.6	0.334440527642153	0.25321377316787763	$1.876796167921135 \times 10^{-7}$
0.7	0.272328715385062	0.19918762605846557	$2.218641400597576 \times 10^{-7}$
0.8	0.197065228326544	0.138449141085021	$5.148130763354963 \times 10^{-8}$
0.9	0.106960690152806	0.07175235809515387	$5.791170627766906 \times 10^{-8}$
1.0	$-9.765920711002352 \times 10^{-13}$	$8.085663848046625 \times 10^{-18}$	$5.607443120337008 \times 10^{-8}$

Ny $= 30;\ \delta = 1;\ H = 1;\ \phi = 0.6;\ G = -1;\ \lambda_1 = 0.2;\ R = 1;\ m = 1$

Table 9: SQLM and Shooting RK4 for Temperature

Y	θ(y)-SQLM	θ (y)- Shooting – RK4	Absolute Error
0	1.066287528908974	1.066287547424466	$1.851549202847024 \times 10^{-8}$
0.1	1.065768213396178	1.0657682295766935	$1.61805153719996 \times 10^{-8}$
0.2	1.064203149333608	1.0642031622300614	$1.289645346069789 \times 10^{-8}$
0.3	1.061568318963338	1.0615683010735861	$1.794597936921604 \times 10^{-8}$
0.4	1.057814314195811	1.0578142863000166	$2.789579434114841 \times 10^{-8}$
0.5	1.052851476059487	1.0528514766537338	$5.94246873930615 \times 10^{-10}$
0.6	1.04652685599369	1.0465267580744422	$9.791924782120986 \times 10^{-8}$
0.7	1.038589938152717	1.0385897992617728	$1.388909443011954 \times 10^{-7}$
0.8	1.028645211531815	1.0286451784135675	$3.311824747775915 \times 10^{-8}$
0.9	1.016085681185261	1.0160856444742878	$2.624048844879212 \times 10^{-8}$
1.0	0.999999999999989	$0.9999999667115499 \times 10^{-18}$	$3.328843911631907 \times 10^{-8}$

Ny $= 30;\ \delta = 1;\ H = 1;\ \phi = 0.6;\ G = -1;\ \lambda_1 = 0.2;\ R = 1;\ m = 1$

Table 10: Convergence for Solid Displacement, Velocity and Temperature

Np	U	V	θ
5	0.2997447935041984	0.3852450995917389	1.0536862034834673
10	0.29990530058383363	0.38479858000289674	1.0528514838665468
15	0.29990530033897844	0.3847985813315716	1.0528514760591237
20	0.2999053003390013	0.3847985813316363	1.0528514760594918
25	0.29990530033900137	0.3847985813316363	1.0528514760594918
30	0.2999053003390014	0.3847985813316363	1.0528514760594918
35	0.2999053003390013	0.3847985813316362	1.0528514760594918
40	0.2999053003390013	0.3847985813316362	1.0528514760594918

Convergence when $\delta = 1; H = 1; \kappa = 0.6; G = -1; \lambda_1 = 0.2; R = 1; m = 1;$

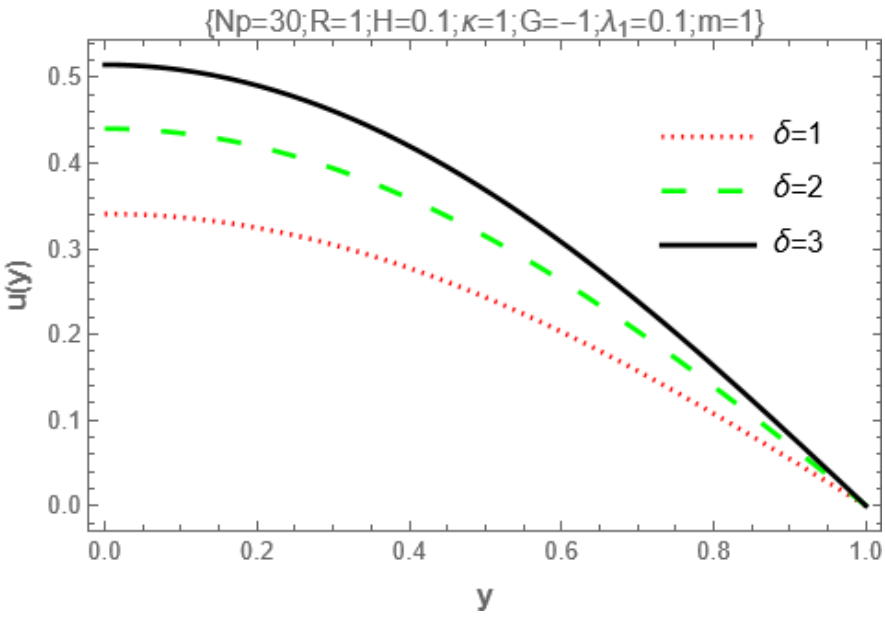

Figure 1: Graph of Solid Displacement with Varying Viscous Drag Parameter

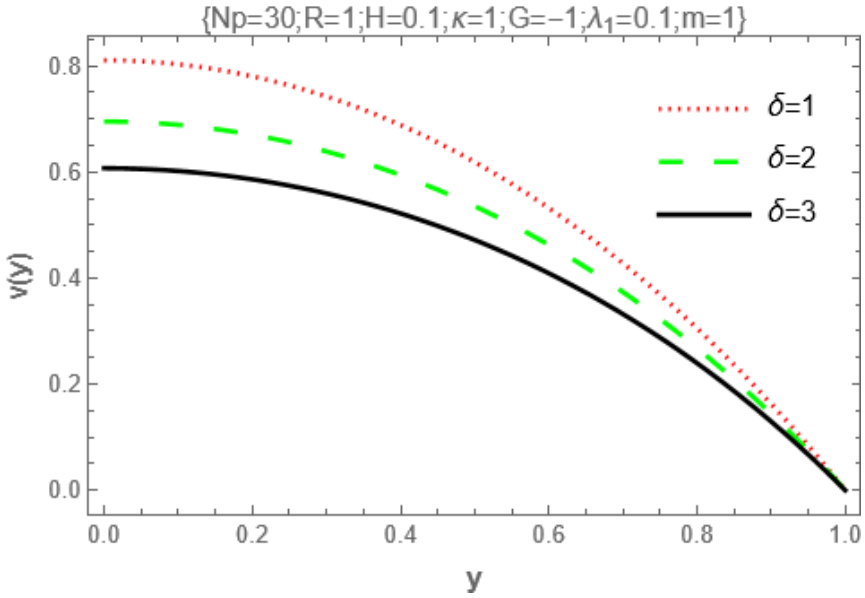

Figure 2: Graph of Velocity with Varying Viscous Drag Parameter

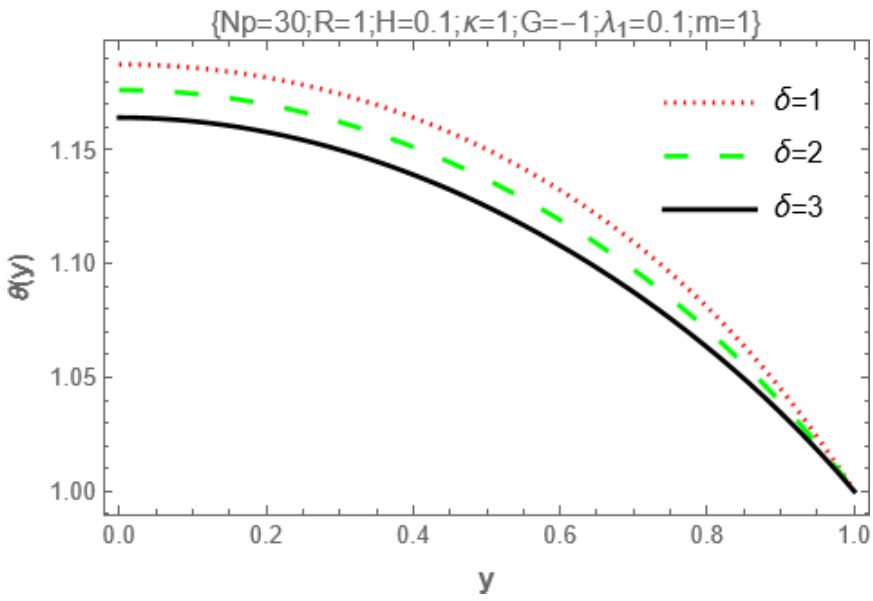

Figure 3: Graph of Temperature with Varying Viscous Drag Parameter

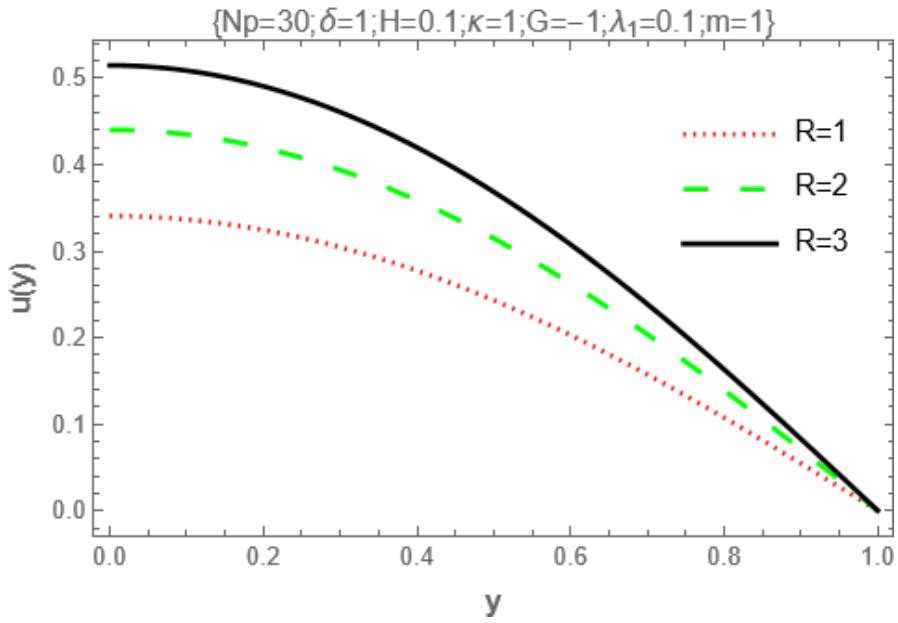

Figure 4: Graph of Solid Displacement with Different Values of Thermal Radiation

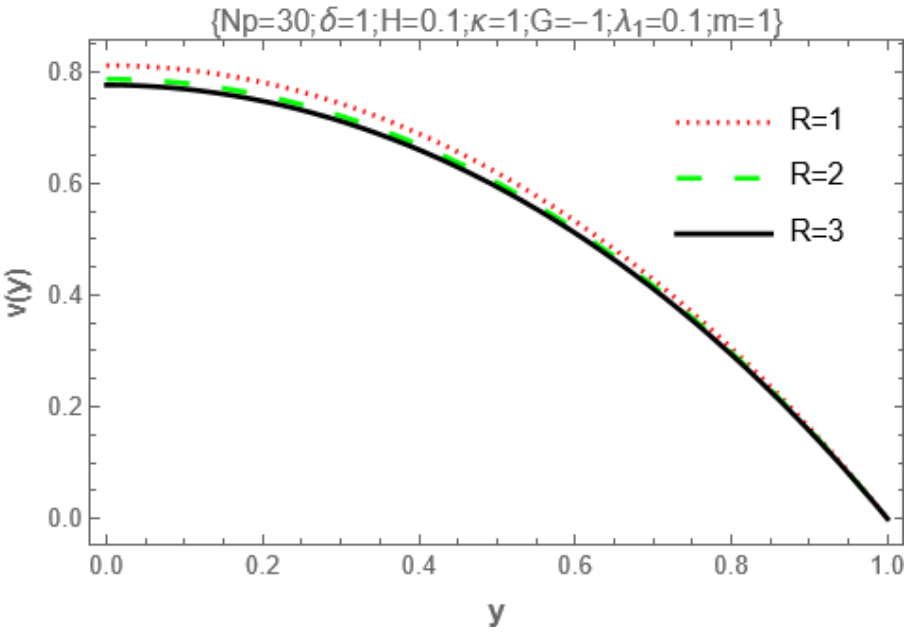

Figure 5: Graph of Velocity with Different Values of Thermal Radiation

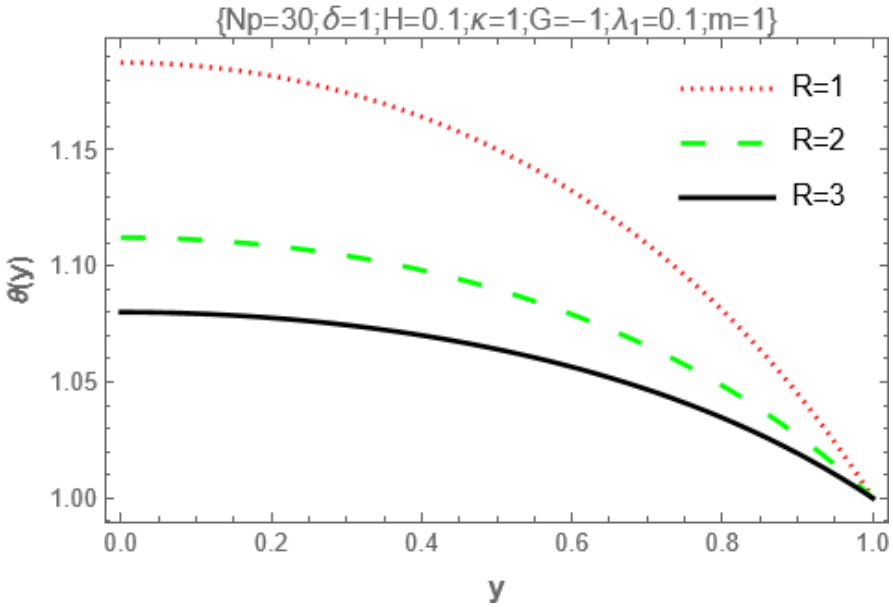

Figure 6: Graph of Temperature with Different Values of Thermal Radiation

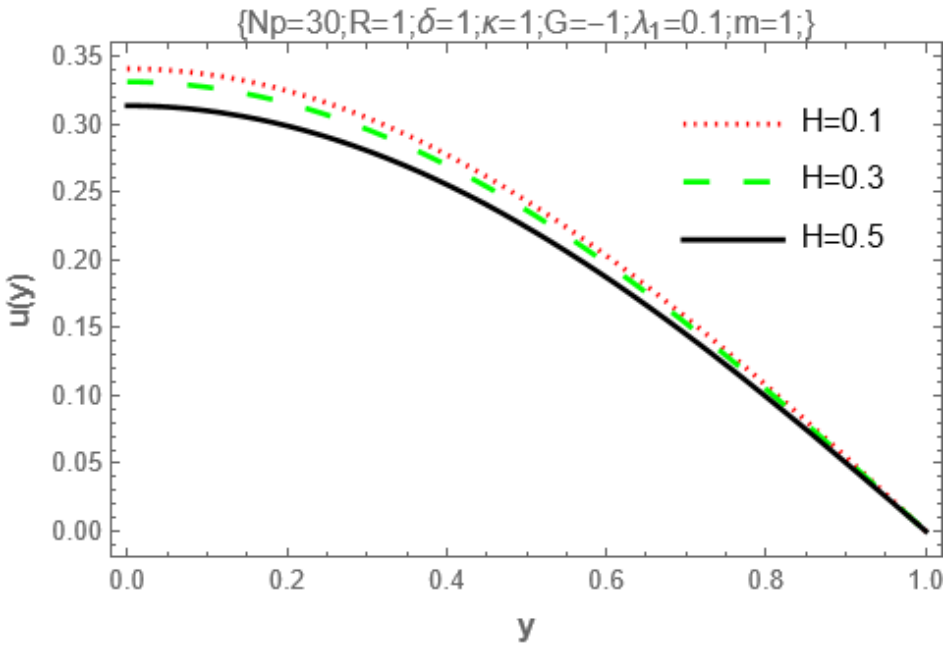

Figure 7: Graph of Solid Displacement with Varying Values of Hartman Number

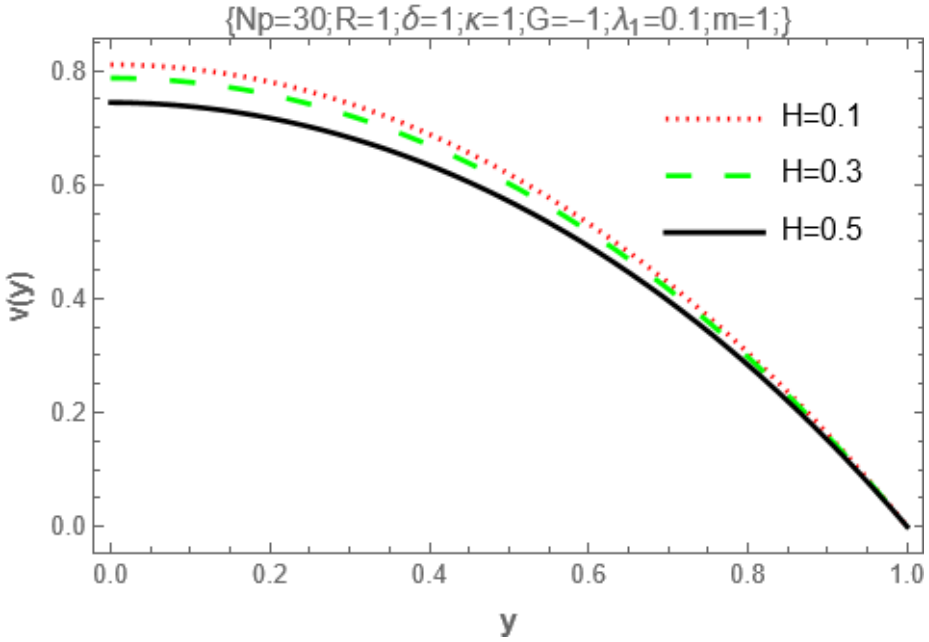

Figure 8: Graph of Velocity with Varying Values of Hartman Number

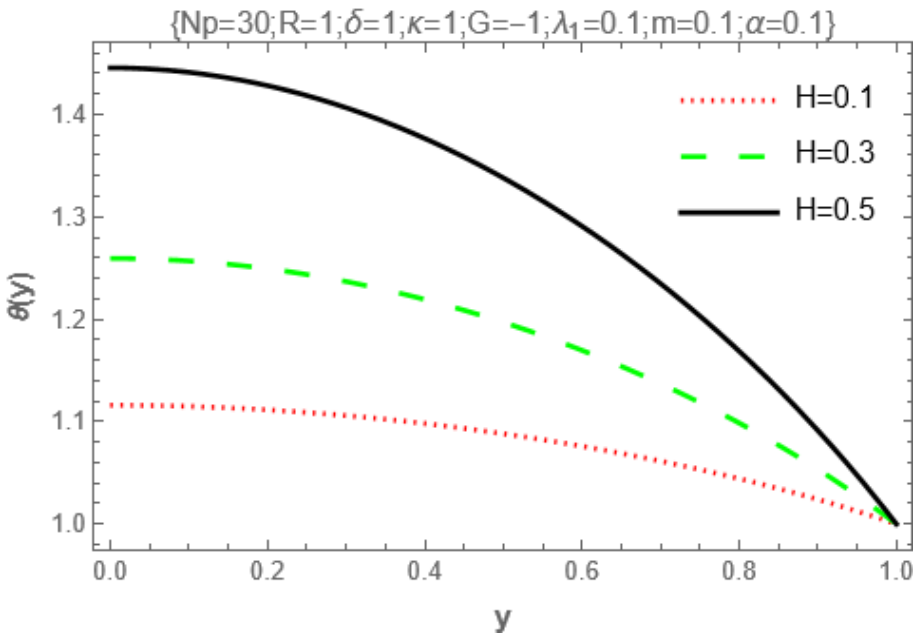

Figure 9: Graph of Temperature with Varying Values of Hartman Number

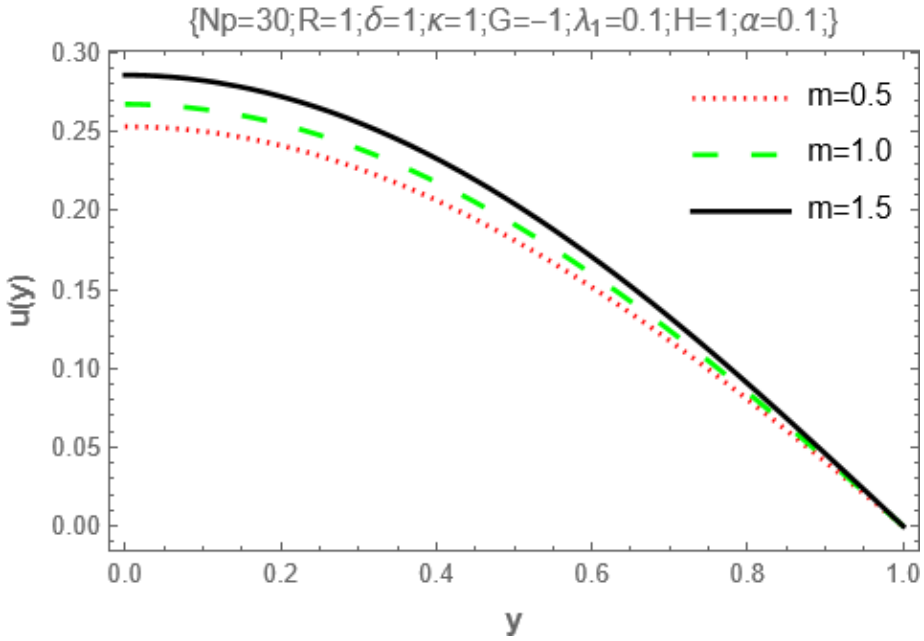

Figure 10: Graph of Solid Displacement with Varying Values of Kinetic Parameter

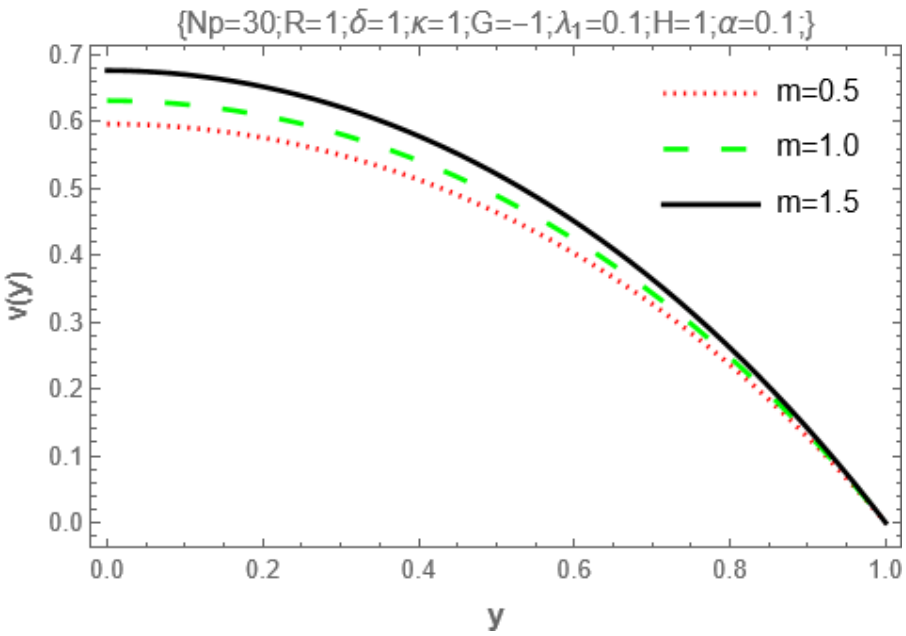

Figure 11: Graph of Velocity with Varying Values of Kinetic Parameter

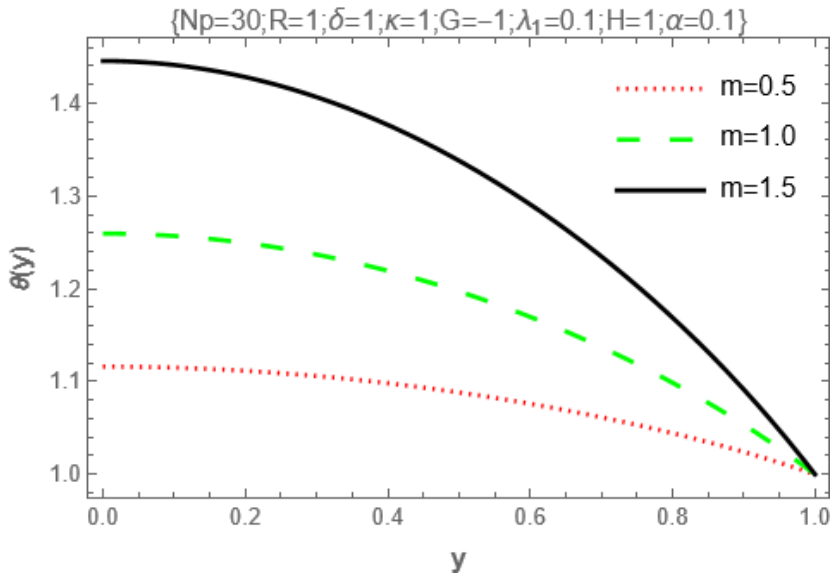

Figure 12: Graph of Temperature with Varying Values of Kinetic Parameter

Figures 1-3 illustrate the velocity (v), solid displacement (u) and temperature (θ) distribution for different values of viscous drag parameter. Figures 4 – 6 illustrate the solid displacement (u), velocity (v) and temperature (θ) distribution for different values of thermal radiation. Figures 7 – 9 illustrate the solid displacement (u), velocity (v) and temperature (θ) distribution for different values of Hartman number. Figures 10 – 12 illustrate the solid displacement (u), velocity (v) and temperature (θ) distribution for different values of kinetic parameter

IV. CONCLUSION

These methods are used to analyze the flow of a viscoelastic biofluid influenced by a magnetic field within a porous, elastic medium. The comparison focuses on the accuracy, efficiency and stability of these methods when applied to the complex mathematical models governing the flow. These comparisons are essential to determine the most suitable numerical approach for accurately predicting the behavior of biofluids in such environments, which has applications in biomedical, engineering, materials science, and other fields where fluid – structure interactions are significant.

REFERENCES

[1] Adesanya S. O., Falade, J. A., Srinivas, J., and Beg, O. A. (2017): Irreversibility Analysis for Reactive Third-Grade Fluid Flow and Heat Transfer With Convective Wall Cooling. Alexandria Eng. J., 56(1), pp. 153-160
[2] Baskaya, M. K., and Cengiz, P. (2005): Neurological and Neurosurgical Intensive Care, Fourth Edition. Pediatric Critical care medicine, 6(4), 502-503. https://doi.org/10.1097/01.pcc.0000167566.64885.92
[3] Bhowmik, H., Tso, C. P., and Tou, K. W. (2005): Analyses of convection heat transfer from discrete heat sources in a vertical rectangular channel. Journal of Electronic Packaging, 127: 215
[4] Biot, M. A. (1941). General Theory of Three-Dimensional Consolidation. Journal of Applied Physics
[5] Biot, M. A. (1956). Theory of Propagation of Elastic Waves in a Fluid-Saturated Porous Solid. Journal of the Acoustical Society of America.
[6] Beg, O. A., Rashidi, M. M., Kavyani, N., and Islam, M. N., (2013): Entropy generation in hydromagnetic convective Von Karman swirling flow, homotopy analysis, Int., J. Applied Math. Mech., 9(4) 37 -65.
[7] Borja, R. I., & Koliji, A. (2009). On the weighted integral and least-squares variational principles for elastoplasticity. Computer Methods in Applied Mechanics and Engineering, 198(30-32), 2221-2236
[8] Choi-Kiwon, S., and Kim, J. S. (1996): Discriminate Sensory Dysfunction after unilateral stroke.Stroke, 27(4), 677-682. https://doi.org/10.1161/01.str.27.4.677
[9] Ermolaev, I. A., and Zhbanov, A. I. (2004): Mixed convection in a horizontal channel with local heating from below. Fluid dynamics, 39(1), 29-35. https://doi.org/10.1023/b:flui.0000024808.33238.ec
[10] Gynaecological Endoscopy, 6(3), 173-176. https://doi.org/10.10461/j.136-2508.1997.98051.x
[11] Gassmann, F. (1951). Elastic waves through a packing of spheres. Geophysics
[12] Khan, N. S., Shah, Z., Islam, S., Khan, I., Alkanhal, T. A., Tlili, I., (2019): Entropy generation in MHD mixed convection non-Newtonian second-grade nanoliquid thin film flow through a porous medium with chemical reaction and stratification, Entropy, 21(2) 139. 35
[13] Kumar, M., Reddy, G. J., RaviKiran, G., Aslam, M. A. M., and Anwar Beg, O., (2019): Computation of entropy generation in dissipative transient natural convective viscoelastic flow in Heat Transfer Asian Research, 1-26, DOI: 10.1002 htj. 21421.
[14] Mallikarjuna, B., Srinivas, J., Gopi Krishna, G., Anwar Beg, O., and Kadir, A., (2021): Spectral Numerical study of Entropy Generation in Magneto-Convective Viscoelastic Biofluid flow through poro-elastic media with thermal radiation and buoyancy effects. . ASME J. Therm. Sci., 011008, pp. 1-12.
[15] Mow, V. C., Keei, S. C., Lai, W. M., & Armstrong, C. G. (1980). Biphastic Creep and Stress Relaxation of Articular Cartilage in Compression. Journal of Biomechanics.
[16] Ramana Murthy, J. V., Anwar Beg, O., Srinivas, J. Ramana Murthy, J. V., (2017): Entropy generation analysis of radiative heat transfer effects on channel flow of two immiscible couple stress fluids, J. Brazilian Soc. Mech. Sci. Eng., 39 2191-2202
[17] Sreenadh, S., Prasad, K. V., Vaidya, H., Sudhakara, E., Gopi Krishna, G., and Krishnamurthy, M., (2016): MHD Couette flow of a Jeffrey Fluid Over a Deformable Porous Layer. Int. J. Appl. Comput. Math., 3(3), pp. 2125-2138.
[18] Stephansson, O. (2003). Rock hydraulics. In Rock Mechanics and Engineering (pp. 139-170).